Exploring the Electronic Structure of Elemental Lithium: From Small Molecules to Nanoclusters, Bulk Metal, and Surfaces

Roger Rousseau[b] and Dominik Marx*[a]

Abstract: Clusters of lithium atoms ranging in size from Li_4 to Li_{40} and bulk metallic solids, including surfaces, are investigated through first principles electronic structure calculations, which are based upon density functional theory and the electron localization function (ELF). It is found that large lithium pπ-type contributions in the electronic wavefunction cause the electrons to localize in interstitial regions, which leads to multicenter bonding for both the clusters and the solids, including their surfaces. For the smaller clusters these stabilizing pπ interactions also lead to short Li–Li interatomic distances, which in conjunction with the longer bonds induces "distance alternation" in the range from 2.45 Å to 3.15 Å. This consequence of the additional pπ interactions is absent in simple solids due to symmetry. The electronic structure of the clusters is topologically insensitive to deformations that do not affect their general shape, but changes significantly upon isomerization. The ramifications upon dynamic properties is that the clusters are quasi-rigid at low temperatures and retain their shape though the distance alternation pattern is suppressed. The picture which emerges for bonding in the bulk solid is that the metallic state arises from the presence of a large number of partially occupied multicenter bonds. For nanoscale clusters only the surface of these clusters exhibits strong localization, whereas their interiors display localization properties similar to the bulk metallic solid. On the other hand, localized states similar to those of the clusters ("dangling bonds") are found on the (001) surface of body-centered cubic (bcc) and face-centered cubic (fcc) lithium solids.

Keywords: bond theory · ELF (electron localization function) · lithium · multicenter bonding · nanostructures

Introduction

Lithium—from molecules to metal: The study of metal clusters ranging in size from a few atoms to a few hundred atoms is an area of research that has seen great activity and progress in recent years.[1–3] Of fundamental interest is how the electronic, structural, and dynamic properties of such aggregates evolve as the number of constituting atoms grows from the molecular regime to the macroscopic scale. This progression in size also represents a crossover in the way the chemical bonds are perceived. For small systems of just a few atoms the well-established concepts of localized chemical bonds in molecules are readily applicable. At the other extreme, the infinite solid also brings with it a well-defined understanding of how bonding occurs.[4, 5] The transition between these two extremes, however, is not well defined and it is not clear how or in what cluster size regime this occurs. This is especially true for metal atoms in which typically the solid-state bonding is thought of as a delocalized rather then a local phenomenon. The evolution of the electronic properties of lithium particles from small molecules to the metallic solid phases has received considerable theoretical attention. Notable theoretical achievements include the McAdon–Goddard rules[6] for the construction of lithium clusters of various sizes; this also provides an intriguing picture of "metallic bonding". Based on Goddard's generalized valence-bond approach it was found that singly occupied orbitals are preferentially localized in interstitial cavities, which are triangles and tetrahedra in the case of planar and compact three-dimensional clusters, respectively. This discovery is intimately connected to the existence of three- and four-center bonds and to the growth pattern that involves packing transitions.[7, 8] The topology of the (total) charge density of *planar* lithium clusters was analyzed in great detail based on correlated wavefunctions.[9] This study finds that the density maxima are preferentially located within triangles formed by three neighboring nuclei, thus giving support to the three-center bonding idea. A complementary analysis that employs the electron localization function (ELF)

[a] Prof. Dr. D. Marx
Lehrstuhl für Theoretische Chemie
Ruhr-Universität Bochum, 44780 Bochum (Germany)
Fax: (+49) 234-321-14045
E-mail: dominik.marx@theochem.ruhr-uni-bochum.de

[b] Dr. R. Rousseau
Steacie Institute for Molecular Science
National Research Council of Canada, 100 Sussex Drive
Ottawa, Ontario, K1N 0R6 (Canada)

  0947-6539/00/0616-2982 $ 17.50+.50/0

of Becke and Edgecombe[10] also reveals the existence of three-center bonds in *planar* lithium clusters.[11] This powerful approach was also used upon the metallic body-centered cubic (bcc) phase of solid lithium. For this metal, as well as others, it is found that metallic bonding is characterized by a three-dimensional network of paths or channels, with essentially constant localization, which connect the points of maximum localization with respect to the ELF.[12] Silvi and Gatti[13] have recently investigated the relationship between the electronic density topology and ELF for several metals including lithium. They found that contrary to previous expectations the metallic bonding does not have a prerequisite of non-nuclear density maxima (as found in lithium clusters). Instead they find that the metallic bond may be viewed as each atom participating in many weak unsaturated covalent bonds. However, this does not address the question of how does the localization pattern evolve from multicenter bonding in finite clusters to the network formation and channeling in the case of extended solids. This aspect belongs to the central themes of the present investigation.

Recently, Pauling's empirical resonating valence-bond theory was applied in a general ab initio implementation to small lithium clusters by McWeeny and co-workers,[14] thereby shining new light on the three-center bonding features of *planar* clusters. This study also highlights the importance of the covalent character of metallic bonding, which involves heavy mixing of the s and p atomic valence orbitals, and, therefore, directionality due to hybridization.[14] The crucial contribution of 2p atomic orbitals to bonding in lithium clusters and the existence of partial sp hybridization was previously emphasized.[7, 9, 15, 16] Another observation concerning the structure of lithium clusters was reported as a side issue in a systematic study of their structure and energetics.[17] The fully optimized structures of various isomers were found to be characterized by the simultaneous presence of long and short Li–Li interatomic distances,[17] for simplicity termed "distance alternation". But the existence of multicenter bonds, p-orbital contributions with significant sp hybridization, and long and short Li–Li distances cannot be unrelated. Furthermore, what role does the p-orbital contribution to the wavefunction play in solid lithium? Naively, one would expect the free-electron picture to hold extremely well for the simplest alkali metal, yet this is not the case. Metallic lithium shows systematic deviations from the free-electron picture of metals in terms of conductivity and Fermi surface-related properties,[18, 19] which can be ascribed to electronic correlation effects.[20–24] However, this also suggests anisotropy in bonding that may result from significant p-orbital contributions in the crystal orbitals. The present paper will close this gap in our understanding by systematically examining the influence of p orbitals upon structure and bonding in both lithium solid and clusters.

Lithium is also the "lightest metal" with an atomic mass of only 6–7 amu Indeed, quantum effects—in particular zero-point motion effects—are known to play a crucial role in determining the ground-state structure of solid lithium[25–29] In addition, it is also well known that the potential-energy surfaces of clusters are rather flat and possess many minima of similar energy.[2] In the limit of low temperatures, quantum-mechanical fluctuations are the dominating excitation mechanism for vibrations of the nuclear skeleton. Early work was devoted to the lithium trimer,[30, 31] followed by a pioneering study[32] of clusters from Li_{20} up to Li_{92} for which strong quantum effects were predicted and culminated in the statement that "the clusters are fluid like at all temperatures",[32] in particular also in the ground state. In the limit of high temperatures thermal fluctuations will dominate over quantum fluctuations. A rich classical–dynamical behavior of clusters was indeed observed in various ab initio molecular dynamics simulations.[3] Issues like melting or packing transitions and isomerization or pseudo-rotation mechanisms and pathways at finite temperatures are of considerable current interest.[7, 33–36] Based on the ab initio path-integral approach to molecular structure calculations,[37, 38] the issue of quantum and classical fluctuations could be settled. It was shown that lithium clusters *do* exhibit significant quantum zero-point fluctuations on the order of magnitude of 100 K thermal excitation[39, 40] Yet this motion is not sufficient to induce fluid-like behavior down to the ground state, at which the clusters remain confined to distinct energy minima so that they maintain their overall "shape". Another significant finding was that the Li–Li distance alternation, which is characteristic for the static optimized clusters,[17] disappears upon inclusion of quantum effects. This means that zero-point motion is strong enough to wash out the bond length differences, whereas it is not sufficient to lead to isomerization reactions; this finding was later confirmed independently.[41] Furthermore, it was briefly alluded to that this behavior is intimately tied with the presence of localized electronic states upon the surface of the cluster.[39] The present study expands upon these aspects and links the behavior of small clusters to that of nanoclusters and finally to bulk surfaces.

As already motivated up to this point, the goal of the present study is to examine and understand the evolution of the electronic structure of lithium ranging from only a few atoms all the way to the extended solid and surfaces. Many previous studies have considered spectroscopic and structural properties of lithium clusters with a fruitful interplay between theory and experiment.[2] In particular, the measured optical spectra of smaller lithium clusters can be well understood in conjunction with electronic structure calculation.[42–44] In the current work the prime interest is the relationship between electronic structure, cluster structure, and dynamic properties. The emphasis is put on understanding the interplay between "localized" and "delocalized electrons" as the assemblies grow and eventually become bulk metal. To this end, we have applied electronic structure calculations based upon density functional theory[45] in combination with topological analysis of the electron density through the electron localization function (ELF).[10]

Computational Methods

Electronic structure calculations: The electronic structure calculations were based upon Hohenberg–Kohn–Sham density functional theory.[45] Local exchange and correlation[46] were supplemented with Becke's exchange gradient correction.[47] The two core electrons were represented by a norm-conserving pseudo-potential,[48] which includes nonlinear core corrections.[49] The remaining valence orbitals were expanded in a 20 au

nonperiodic cubic box by using plane waves with a kinetic energy cutoff of 30 Ry (except in the case of Li_{40} where the box length was 42 au and for the bulk phases and surfaces of metallic lithium for which the cutoff was 20 Ry, see below for details). The overall approach gave excellent results not only for the cluster structures, but more importantly for the crucial energy differences between various isomers of a given cluster, see refs. [17, 40] for a detailed analysis of these issues. All calculations were carried out with the ab initio molecular dynamics package CPMD.[50]

The structures up to Li_{20} were taken from our previous studies.[17, 39, 40] The structure of the Li_{40} cluster was obtained by performing a 2 ps Car–Parrinello molecular dynamics simulation[51] at 500 K within a 42 au cubic cell and 15 Ry plane wave cutoff. The initial structure was obtained by taking a $3a \times 3b \times 2c$ segment of the bcc lithium structure with an additional four capping atoms in the c direction to create as isotropic a distribution of atoms as possible. This was followed by simulated annealing down to a temperature below 10 K over a period of another 1 ps. In order to check this result, the procedure was repeated (randomization of atomic positions, heating, molecular dynamics, annealing) resulting in a final cluster that was only 2 kcal mol^{-1} lower in energy; this indicates that structures obtained from this procedure are located within low-lying energy basins of the potential-energy surface. In a final step residual forces were removed by local geometry optimizations. All cluster structures discussed in this work have been characterized by stationary-point analysis of the potential-energy surface and are local minima. Note that although we are confident that low-energy configurations were obtained even for the two largest clusters, we do not in any way presuppose that these are the *global* minima on the potential-energy surface.

Having obtained the real-space structures, the electronic structure was reoptimized at a higher cutoff (20 Ry for Li_{40} and 30 Ry for all other clusters) in order to calculate the ELF. This cutoff, which is larger than the one required in order to converge structures and energies,[40] assures a smoother representation of the Kohn–Sham orbitals for the purpose of the electronic structure analysis.

The calculations of bulk lithium were performed within the framework of fixed-volume supercell calculations with the Γ point of the Brillouin zone. In conjunction with large supercells, this amounts to a sufficient sampling of **k** points in the Brillouin zone of the primitive cell, vide infra. For simplicity, only the body-centered cubic (bcc) and face-centered cubic (fcc) phases are considered, fcc being a representative of close-packed structures. In particular, a $5a \times 5b \times 5c$ cubic supercell (250 atoms, $a = 3.51$ Å) for bcc and a $4a \times 4b \times 4c$ cubic supercell (256 atoms, $a = 4.41$ Å) for fcc have been used with lattice constants taken from experiment.[52] In order to investigate surfaces, the (001) surface of both bcc and fcc solids were used. These calculations were based on a $4a \times 4b \times 4c$ (128 atoms, thickness ten atomic layers) slab for bcc and a $2a \times 2b \times 2c$ (120 atom, thickness eight atomic layers) slab in the case of fcc. The slabs were separated by a 10 Å vacuum region. Structure relaxation for only those atoms residing on the upper two atomic layers were conducted by simulated annealing from 50 K to temperatures below 5 K. All bulk and surface calculations were performed with a 20 Ry energy cutoff.

Electronic structure analysis: The analysis of the electronic structure and bonding has been carried out mainly using the electron localization function (ELF)[10] supplemented by its topological bifurcation analysis.[53] Several excellent review and research papers discuss in depth the foundations, properties, and interpretations of the ELF[12, 54–58] so that only a concise presentation is required here. The ELF can be viewed as a local measure of the Pauli repulsion between electrons owing to the exclusion principle in three-dimensional space. It therefore makes it possible to define regions of space that are associated with different electron pairs in a molecule or solid. The definition of ELF is given by Equations (1)–(4),

$$\eta(\mathbf{r}) = \frac{1}{1 + (D_P/D_h)^2} \quad (1)$$

$$D_P = \frac{1}{2}\sum_{i=1}^{N} |\nabla \psi_i|^2 - \frac{1}{8}\frac{|\nabla\rho|^2}{\rho} \quad (2)$$

$$D_h = \frac{3}{10}(3\pi^2)^{2/3}\rho^{5/3} \quad (3)$$

$$\rho = \sum_{i=1}^{N} |\psi_i(\mathbf{r})|^2 \quad (4)$$

whereby the sum is over all singly occupied one-electron (spin-) orbitals $\psi_i(\mathbf{r})$ in a N-electron system.

The ELF is normalized between zero and unity and its value for the homogeneous electron gas—a well-defined reference state—is 1/2. Note that Equation (1) reduces to the trivial solution $\eta(\mathbf{r}) \equiv 1$ for two-electron systems, such as, in particular, Li_2 or Li_3^+ if only the valence electrons are taken into account. The function $\eta(\mathbf{r})$ is large in spatial regions in which the Pauli repulsion $\sim D_P(\mathbf{r})$ is small, that is, where two electrons with antiparallel spin are paired in space. This can be understood by interpreting the full-space integral $\int d\mathbf{r}\, D_P(\mathbf{r})$ of the two additive terms that constitute D_P in Equation (1), see refs. [12, 54, 56] and references cited therein for the underlying work. The integral of the first term is the total kinetic energy of N noninteracting *fermions* in the ground state, whereas that of the second term is minus the kinetic energy of the corresponding *bosonic* system. The latter is a lower bound for the former so that $\int d\mathbf{r}\, D_P \geq 0$. Both kinetic energies correspond to those of indistinguishable particles, the only difference being that in the fermionic case the antisymmetrization induces a nodal structure of the ground-state wavefunction that increases the curvature of the orbitals and, thus, the total kinetic energy. In contrast, the bosonic N-particle ground-state wavefunction and, therefore, its density is built from a single orbital for all N particles. If analogous arguments are invoked locally by using $D_P(\mathbf{r})$ instead of its integral, it becomes evident that D_P quantifies the "amount of Pauli repulsion" at a given point **r** in space. As a result, this excess Pauli kinetic energy is expected to be small in a region in which a pair of electrons with opposite spin states is localized. As a result of the particular normalization chosen, this means that η approaches unity in these regions. Conversely, the Pauli energy is large in a region in which two or more of these electron pairs approach each other. A complementary description in terms of the orbitals nodes and a link to the orbital picture of bonding is worked out in ref. [57], and the connection to Bader's analysis in terms of the Laplacian of the density is established in ref. [56].

The location of the maxima of $\eta(\mathbf{r})$ with values denoted by η^{max} are attractors because other points in space can be connected to them by maximum-gradient paths. The set of all the points in space that were in this sense "attracted" by one special point define the basin of that particular attractor. In addition, higher η^{max} values correspond to more tightly localized electron pairs in space and as such may be used as an indicator to discriminate different bonds. If the electron density is integrated over a given basin, the corresponding number can be interpreted as the number of electrons that are involved in that particular bond. In general, there is more than one attractor present for a N-electron system and thus more than one basin. The set of those ELF values for which a given basin just merged with another one, the bifurcation value η^*, is another set of characteristic numbers. The so-called bifurcation diagram results from connecting successively on a descending ELF scale every attractor maximum with its bifurcation values until finally all attractors are connected; this corresponds to the situation in which all electrons are contained in one large domain encompassing the entire system. Analyzing the topology of the electronic structure in terms such "bifurcation hierarchies" is a valuable method in order to compare the bonding characteristics of various systems with each other.[12, 53] Finally, it is worth noting that the present ELF and charge density analyses are based exclusively on the chemically relevant valence electrons, thus leaving out the "trivial attractors" due to the core localization.

Results and Discussion

The molecular realm

From Li_2 to Li_5^+—three-center and four-center two-electron bonds: The first non-trivial candidates to discuss are the Li_4 and Li_5^+ molecules or "clusters". The structure of the lowest energy isomer of Li_4 is that of two edge-sharing triangles, both of which lie in the same plane (D_{2h}), see Figure 1a. This molecule may be described as containing one short Li–Li distance of 2.58 Å across the center of the cluster, and four equivalent long ones of 3.00 Å located along the outer edges. In general an Li–Li interatomic distance is classified to be "short" or "long" if it is in the range 2.40–2.80 Å or 2.80–

0947-6539/00/0616-2984 $ 17.50+.50/0 *Chem. Eur. J.* **2000**, *6*, No. 16

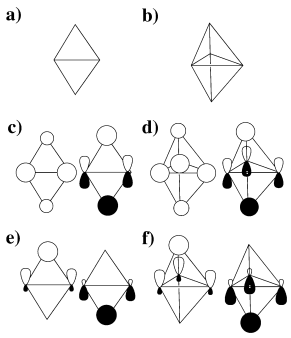

Figure 1. Structure of the ground state isomers of a) Li_4 and b) Li_5^+. The lithium positions (vertices) are connected by lines. Schematic representation of c),d) the two occupied canonical Kohn-Sham valence orbitals, and e),f) the corresponding localized orbitals of both clusters, respectively. In panels c) and d) the left and right subpanels correspond to the lowest wand highest occupied orbitals, respectively. Empty, filled regions of the orbitals distinguish their sign in the respective region.

3.20 Å,respectively. For reference purposes, note the bond lengths of 2.65 Å and 2.90 Å for Li_2 and Li_3^+, which are ideal representatives of two-center two-electron and three-center two-electron bonding cases, respectively. Previously, it has been reported[6, 9, 11, 14, 15] that the electrons are localized within the center of the two triangles in Li_4 thereby forming two three-center two-electron bonds; the electron density of the Li_2 molecule was analyzed in detail in several studies.[59] Also in the case of the lowest energy isomer of Li_5^+ with its trigonal bipyramidal shape, see Figure 1b, the two distinct types of distance, short and long, are present. The three Li–Li contacts along the equator of the bipyramid are found to be short, 2.70 Å, whereas the six to the atoms capping the triangle are long, 3.15 Å. Previous studies[6, 15] again find that there are two multicenter bonds, each containing a pair of electrons within the center of a distorted tetrahedron. Thus, Li_5^+ may be considered as consisting of two four-center two-electron bonds, which are face-sharing across the equator of the bipyramid.

To understand how these findings come about it is appropriate to start this examination with the canonical Kohn – Sham orbitals drawn schematically in Figure 1c and 1d for Li_4 and Li_5^+, respectively. These orbitals are obtained by projection of the plane-wave basis set upon a localized (minimal atomic) basis derived from the pseudo-wavefunction. The lowest energy orbitals contain only lithium s-type character for both clusters, see the left subpanels in Figure 1c and 1d. However, this is not true for the remaining orbital, which is found to have a substantial ($\approx 25\,\%$) p-type character, see the right subpanels in Figure 1c and 1d. This large p-orbital contribution has been highlighted previously in various reports[7, 9, 14, 15, 16], but without connecting this finding to the distance alternation and multicenter bonding features.

How is the large p-orbital contribution related to the distance alternation? The orbital representation in Figure 1c and 1d makes clear this point: in Li_4, the p-orbitals "act in phase" across the short Li–Li contact thereby creating an extra π-like bonding interaction. This fits well with the observed contraction of the associated Li–Li distance, which is even shorter than that of Li_2. The same is true for Li_5^+: the presence of p-orbital contributions in the highest occupied Kohn – Sham orbital leads to a stabilizing π-bonding interaction across the equator of the cluster and explains the shrinkage in the equatorial plane to a length close to that in the dimer. Thus, the distance alternation can be explained naturally by a p-orbital contribution to the molecular wavefunction, which leads to an additional stabilization and thus shortening of the involved interactions.

How does this relate to electron localization? The canonical Kohn – Sham orbitals can easily be transformed to obtain localized orbitals as is illustrated schematically in Figure 1e and 1f for Li_4 and Li_5^+, respectively. Based on these orbitals, the valence charge density can be redistributed into two three-center two-electron bonds (localized in the upper and lower triangle) for Li_4 and two four-center two-electron bonds (localized in the upper and lower tetrahedron) for Li_5^+, see the left and right subpanels for each case. The directionality of the p-orbital is essential in this explanation, because without being able to form the sp-hybrid orbitals at the atoms that interface the two triangles or tetrahedra, this transformation would not yield these simple bonding patterns.

The topology of the electronic structure of Li_4 and Li_5^+ can also be examined in the language of the electron localization function (ELF) as defined in Equation (1). This is a truly complementary approach as orbital hybridization schemes are nonunique, whereas the interpretation of the ELF might not always be evident at the outset. The ELF analysis can be performed graphically by plotting isosurfaces with $\eta(\mathbf{r}) = \eta^{\mathrm{iso}}$ of this scalar function in three-dimensional space like the ones shown in Figure 2a and 2b for Li_4 and Li_5^+, respectively. In this

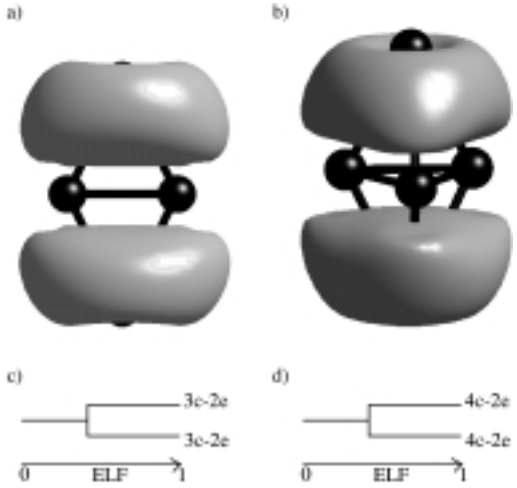

Figure 2. ELF isosurfaces at $\eta^{\mathrm{iso}} = 0.9$ for a) Li_4 and b) Li_5^+. The lithium positions are marked by black balls, which are connected by sticks to guide the eye. The ELF bifurcation hierarchy is represented in diagrammatic form in c) and d) for Li_4 and Li_5^+, respectively. Labels on the bifurcation diagrams are: 3c-2e three-center two-electron bond; 4c-2e four-center two-electron bond.

representation, the attractors and their basins are rendered evident by visual means. Both clusters show two degenerate attractor basins with strong electron localization, that is, $\eta^{\max}$ is very close to unity. In the case of Li_4, both basins (with the ELF maxima in the center of the triangles) contain two electrons that are shared between three centers, whereas four centers are held together by two electrons in the Li_5^+ case (with one attractor in the *center* of each tetrahedron). Note

that the short Li–Li bonds are situated in regions of low ELF values, that is, *between* the attractor basins, which is a direct consequence of the π-bonding contribution. The bifurcation value for which the two attractor basins are confluent and form one basin that contains all electrons occurs at a well-separated value of about $\eta \approx 0.5$ for both cases. This is represented schematically in Figure 2c and 2d by the use of bifurcation diagrams.[53] In this diagram the maxima of ELF are represented by the terminus of a branch on a tree diagram and the bifurcation value is represented by the merging of two branches. The independence of the three-center and four-center bonds as found in Li_4 and Li_5^+, respectively, is well reflected by the large separation between the values of η^{max} and η^* as seen in the bifurcation diagram of Figure 2c and 2d. Thus, the topological ELF analysis substantiates the earlier finding that Li_4 is bound by two three-center two-electron bonds, whereas Li_5^+ is best described by two four-center two-electron bonds. One distinct advantage of using ELF to analyze bonding over other schemes is that multicenter bonds can easily be located graphically "by inspection" of ELF isosurfaces.

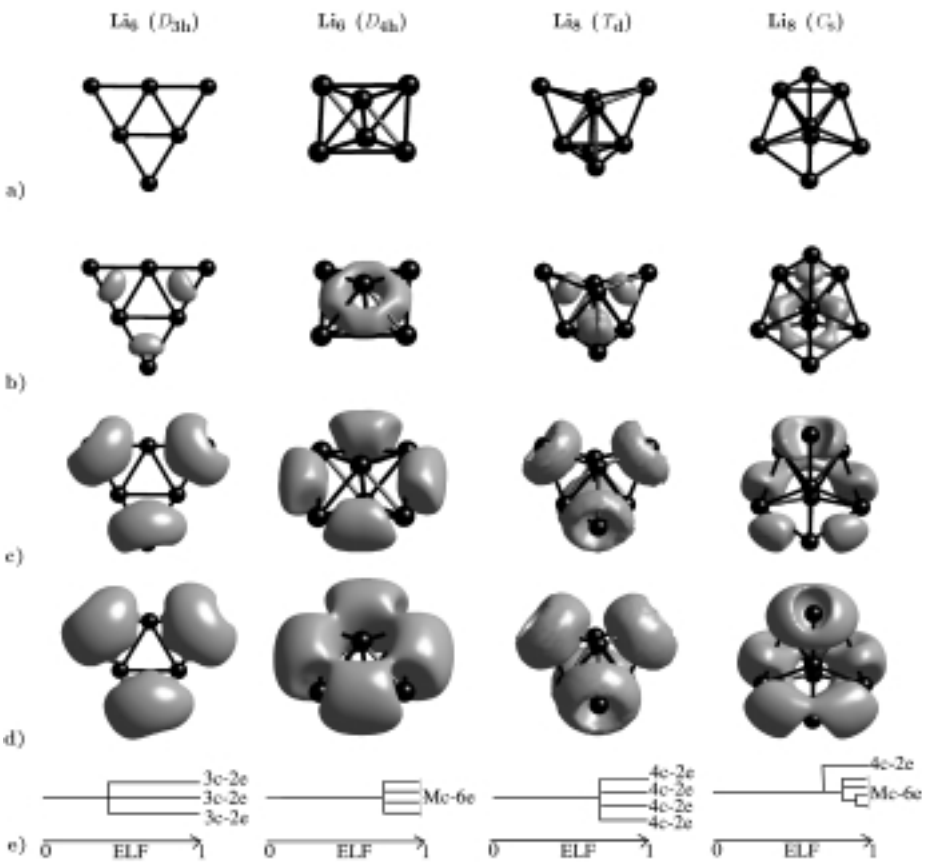

Figure 3. a) The structures of the planar D_{3h} and three-dimensional D_{4h} isomers of Li_6 and the T_d and C_s isomers of Li_8. The corresponding valence charge density isosurfaces at $\rho^{iso} = 0.85\rho^{max}$ (ρ^{max} denotes the value of the absolute maximum of the valence charge density) are shown in b) for each cluster, and the ELF isosurfaces at $\eta^{iso} = 0.9$ and $\eta^{iso} = 0.8$ are shown in c) and d), respectively. Schematic bifurcation diagrams are shown in e) for ELF of each cluster. Labels on the bifurcation diagrams are: 3c-2e three-center two-electron bond; 4c-2e four-center two-electron bond; Mc-6e multicenter six-electron bond.

Planar and nonplanar Li_6—from three-center two-electron to multicenter bonding: Next, consider a slightly larger, but as it will turn out much richer case: Li_6 with two distinctly different isomers as depicted in Figure 3a. The first isomer is the well-known planar D_{3h} structure, which has only longer Li–Li distances in the range 2.97 – 3.00 Å. The second isomer is an octahedron that is subject to axial compression, which results in a structure with D_{4h} symmetry. Overall, this isomer contains nine short Li–Li distances, eight of 2.80 Å from the axial positions to the four atoms in the central plane, and the unusually short central Li–Li distance of only 2.47 Å (cf. 2.65 Å in Li_2). The former of these two isomers has been the subject of intense study,[6, 9, 11, 14, 15] whereas the latter one has received attention only recently.[17, 35] This is despite the fact that it is clearly much lower in energy by about 5 kcal mol^{-1} as carefully assessed in ref. [17] based on various methods, see Table 7 therein. The planar D_{3h} structure is known to contain three three-center two-electron bonds,[6, 9, 11, 14, 15] but what of the more stable D_{4h} isomer?

To this end, we compare the isosurfaces of the (valence electronic charge) density $\rho(\mathbf{r})$ with the ELF (Figure 3b and 3d, respectively). In accord with previous studies[6, 9, 14] we find for the planar D_{3h} isomer the density located predominantly within the three outer triangles of the cluster, Figure 3b. As in ref. [11], the ELF provides three strong attractor basins (with maxima in the centers of the three outer triangles) that can easily be associated with three three-center two-electron bonds, see Figure 3c and 3d. The ELF bifurcation diagram in Figure 3e shows that the three two-electron attractor basins are confluent at a well-separated value of $\eta^* \approx 0.47$; this indicates that these attractor basins can truly be thought of as three independent localized bonds. The resulting bond lengths of 2.97 – 3.00 Å also compare well with the ideal three-center two-electron bond in Li_3^+ with a reference length of 2.90 Å.

Before examining the ELF of the nonplanar D_{4h} isomer, it is instructive to consider first the occupied canonical Kohn–Sham orbitals as represented in Figure 4a and 4b for the D_{3h} and D_{4h} species, respectively. Inspection of these orbitals indicates that here also there is significant (≈20%) p-orbital character present in the highest occupied molecular orbitals. Most importantly, the central Li–Li interaction of the D_{4h} isomer contains not only the s-orbital contributions, but *two* orthogonal p orbitals on the two lithium atoms that terminate this short bond contribute to an extra π-type interaction. This leads to a situation that would conventionally be considered as a "triple bond", compare with the standard orbital picture

0947-6539/00/0616-2986 $ 17.50+.50/0 *Chem. Eur. J.* **2000**, *6*, No. 16

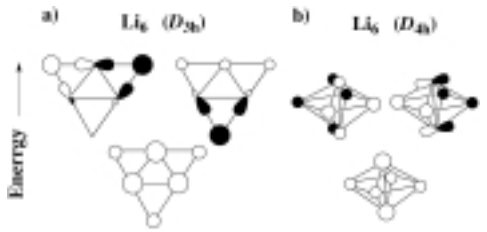

Figure 4. Schematic representation of the the canonical valence orbitals of a) the planar D_{3h} and b) three-dimensional D_{4h} isomers of Li_6. Note that for the D_{4h} isomer the orientation is such that here the central short bond lies in the paper plane, which differs from that chosen for Figure 1a. For symbols see caption of Figure 1.

of carbon–carbon triple bonds. Furthermore, there is no such π-bonding interaction for the planar D_{3h} isomer. As such, the planar isomer not only has longer Li–Li distances, but it is also less stabilized by π-bonding which is precisely the reason why the D_{4h} isomer is much lower in energy. One important ramification of this finding is that the two-dimensional → three-dimensional packing transition[7, 8] of these clusters can be related to the number of additional p-orbital interactions in compact three-dimensional versus planar structures when the clusters grow.

In stark contrast to the planar isomer, the density of the three-dimensional Li_6 isomer has, interestingly, a ring of enhanced density around the central short Li–Li bond, see Figure 3b. This, together with the extremely short distance of only 2.47 Å and the result of the orbital analysis, strengthens the notion of a stabilizing "triple bond" character in this Li–Li bond. This gets further support from the ELF analysis: there are *four* attractor basins (with strong maximum localization: $\eta^{max} \approx 1.0$) which form along the outside of the cluster, see Figure 3c and 3d. The corresponding attractors peak in the equatorial plane, with their maxima just *outside* the Li–Li connecting lines, that is, in a region in which the charge density is very small. Unlike the well-separated attractor basins of the D_{3h} isomer, those in the D_{4h} isomer already merge into one basin at a much higher value η^* on the normalized ELF scale, see Figure 3e. These four basins collapse at a bifurcation value of $\eta^* = 0.86$ into a single *ring*, which is hosted in the region of sufficient charge density. Such ring-type basins in ELF topologies have been seen for compounds like acetylene with triple bonds,[54] (see in particular Figure 2g and 2h in this reference) and it is tempting to invoke a similar interpretation here. However, to do this would amount to ignoring the fact that there are indeed four distinct attractor basins that may each be ascribed 1.5 electrons by symmetry. These so-called *unsaturated* attractor basins are characteristically found in molecules such as benzene, which have multiple resonance structures, or in metals. Although the ring feature is clearly indicative of triple-bonding character in the 2.47 Å bond, it is more meaningful to describe this as a more delocalized multicenter six-electron bond, rather then a two-center six-electron bond as in acetylene. This behavior of ELF reflects the fact that delocalization of electrons is a meaningful energetic alternative to "discrete" two-electron bonds in the case of small lithium clusters.

In summary, the Li_4, Li_5^+, and planar Li_6 (D_{3h}) clusters are examples in which the complex bonding scenario may be thought of as consisting of the "additive" interaction of several independent localized *two*-electron bonds, albeit of a multicenter nature. The nonplanar D_{4h} isomer of Li_6, on the other hand, does not fit into this simple picture, but is suggestive of bonding in a more global sense, which accords better with the concept of a cluster being "on its way to the solid". This example also brings to the surface a rather tantalizing question to ponder: "is this decrease in the energetic preference for independent two-electron bonds an early symptom of the metallic character?"

Li_8—perturbing the ideal bonding pattern: The logical next step consists of adding more electrons to see if delocalized multicenter bonding is generic, or a specific occurrence for Li_6 only. Toward this end two isomers of Li_8 were examined, see Figure 3a. The lowest energy isomer consists of a tetrahedron with each of its four triangular faces capped by another lithium atom giving the molecule an overall T_d symmetry. The Li–Li distances between atoms in the central tetrahedron are 2.88 Å and those to the capping atoms are 2.94 Å. These tetrahedral subgroups are reminiscent of Li_5^+, which was composed of two four-center two-electron bonds. A second low-energy C_s isomer of Li_8 was obtained from elaborate ab initio simulated annealing in our previous studies[39, 40] and is also depicted in Figure 3a. It is only 0.3 kcal mol^{-1} higher in energy than the T_d isomer, which is beyond the accuracy of the currently used electronic structure methodology to reliably distinguish. Its C_s structure is that of a pentagonal bipyramid with one of the triangular faces capped by an additional atom with Li–Li distances up to 3.10 Å. Most notable for the present purpose is again the existence of a short Li–Li distance (2.74 Å) that cuts across the center of the cluster, reminiscent of the central bond in the D_{4h} isomer of the Li_6 cluster. These two very different but energetically quasi-degenerate structures provide a perfect opportunity to examine in detail how multicenter bonds behave in larger clusters.

The charge density of the T_d isomer is piled up within the outer tetrahedral subgroups, whereas the central tetrahedron has essentially no density within it, Figure 3b. This cluster may then be thought of as consisting of four four-center two-electron bonds, thereby extending the bonding and packing schemes introduced by Li_5^+ to larger systems. The ELF (Figure 3c and 3d) reflects this with the presence of four strong attractor basins $\eta^{max} \approx 1.0$ that remain isolated from each other down to a bifurcation value of $\eta = 0.76$ where they merge outside of the cluster in regions of low electron density. This value is significantly lower than in the nonplanar Li_6 case, but also higher than for Li_4, Li_5^+, and planar Li_6. This signals already an attenuation of the independence of these bonds.

The scenario of the C_s isomer is distinctly different concerning both density and ELF (Figure 3b and 3d). The charge density (Figure 3b) reveals a distorted ring within the pentagonal bipyramid, much like that found in nonplanar Li_6. In addition, there is a pile up of density within the outer tetrahedral subgroup involving the capping atom, much like those found within the T_d isomer. The ELF is characterized by five attractor basins: four on outer edges of the pentagonal

  0947-6539/00/0616-2987 $ 17.50+.50/0

bipyramid (with a maximum localization of $\eta^{max} = 0.98$) and one within the tetrahedral subgroup ($\eta^{max} = 0.97$). The former group of four basins collapses into a single distorted ring already at a value of $\eta^* = 0.88$, which is close to the value $\eta = 0.86$ in nonplanar Li_6. In contrast, the attractor basin around the capping atom remains isolated down to a significantly lower value of $\eta^* = 0.75$, which is close to the value $\eta^* = 0.76$ in its T_d isomer. Hence, the bonding within this cluster can be described as consisting of a multicenter six-electron bond in the core (similar to that of nonplanar Li_6) and a four-center two-electron bond that involves the capping site (similar to the T_d Li_8 isomer). For the Li_8 clusters multicenter bonds are energetically comparable with four-center two-electron bonds. This further strengthens the point about delocalized bonding within clusters as being an important step toward bonding in the bulk metal.

Implications—fluctuations, dynamics, and properties: What are the ramifications of the multicenter bonding upon isomerization reactions, dynamics, and general properties of these clusters? A simple representation of the electronic structure as provided by the one-component plasma model,[32] which does not account for the multicenter bonding, underestimates cluster rigidity. In particular, it leads to a too soft (fluid-like) dynamic behavior at low temperature as compared with ab initio path-integral simulations.[39–41] To further probe these questions the cluster structure of the Li_8 C_s isomer was "shape-consistently perturbed" by artificially changing all the Li–Li distances such that they all have the same (average) length of 2.98 Å. As a result, the distance alternation is destroyed, whereas the general shape of the cluster is preserved, see Figure 5a. In comparison with the optimized C_s structure, see Figure 3e, we find an *identical* pattern for the ELF in terms of its topology. Furthermore, there is quantitative agreement: compare Figure 5c and 5e as well as the bifurcation diagram in Figure 5g with the respective panels in Figure 3. This model calculation is confirmed by using more realistically distorted structures sampled from ab initio molecular dynamics trajectories[40] that were generated at finite temperatures. As long as the cluster maintains its overall shape, the electronic structure is found to be rather insensitive to the precise positions of the ions.

To understand how this may transpire it is worth noting that both the 2s and 2p atomic orbitals of the lithium atom are extremely diffuse with radial maxima at about 1.6 Å from the nucleus. These diffuse orbitals lead to substantial overlap even at large inter-nuclear separations with a weak distance dependence. For example, the overlap between two Li 2s orbitals decreases by only $\approx 10\,\%$ as the inter-lithium distance increases from 2.50 Å to 3.10 Å. Likewise, the 2p–2p π overlap drops by about 13 % over the same range. As a result, the change in the wavefunction as bonds are stretched or contracted will be minimal and, hence, the ELF will be relatively insensitive to small fluctuations of the underlying cluster structure.

This is no longer true if the cluster shape itself changes. To make clear this point consider a model "isomerization reaction" in which the tetrahedral capping group of the C_s isomer of the Li_8 cluster is transmuted into a triangle, see

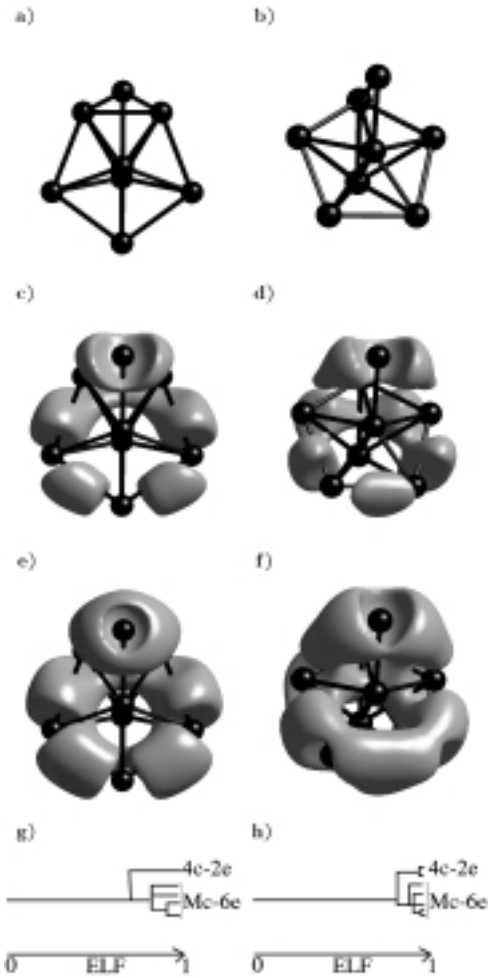

Figure 5. Structure of Li_8 clusters derived from the C_s minimum structure (see Figure 3a): a) distortion where all distances equally long with 2.98 Å and b) a transition state. ELF isosurfaces are depicted in c) and d) for $\eta^{iso} = 0.9$ and in e) and f) for $\eta^{iso} = 0.8$ for both isomers. ELF bifurcation diagrams are depicted in g) and h), see caption of Figure 3 for nomenclature.

Figure 5b and 5h for the involved optimized transition state, which is about 0.7 kcal mol^{-1} higher in energy then the C_s isomer. The ELF changes its topology and now features seven attractor basins (with $\eta^{max} = 0.98 - 0.97$) instead of five as before. The two basins around the capping triangle are found to merge *first* at $\eta^* = 0.96$, followed by the collapse of the five basins within the bipyramid into a distorted ring at $\eta^* = 0.90$, and the final confluence occurs at $\eta^* = 0.88$. This bifurcation hierarchy (see Figure 5h) and, thus, the chemical bonding is *qualitatively* different from that of the more stable isomer (see Figure 3e) and its "shape-consistent distortion" (see Figure 5g). Changing the cluster shape leads to grossly different electron localization properties.

What are the implications of these findings for the dynamic behavior, or in other words, what is the effect of "fluctuations" on the potential-energy surface? These fluctuations might be of thermal and/or quantum-mechanical origin, such as zero-point motion or tunneling for a relatively light nucleus as lithium. Independently, we and another group have assessed previously[39–41] these effects in Li_8 and Li_{20} using finite-temperature ab initio path-integral simulations[37, 38], that take also the quantum nature of the nuclei into account. In "cold"

0947-6539/00/0616-2988 $ 17.50+.50/0 *Chem. Eur. J.* **2000**, *6*, No. 16

clusters at 10 K, it was uncovered that quasi-harmonic zero-point motion in lithium clusters is quite large and leads to root-mean-square bond-length fluctuations of about 5%, whereas tunneling is negligible. Such motion does eliminate the distance alternation, that is, the distinction between short and long Li–Li distances, but it does not lead to isomerization; the same is true for thermal fluctuations at about 100 K. However, this picture breaks down for "hot" clusters with internal temperatures of several hundred Kelvin, for which, in general, a rich dynamic behavior is found.[33–36]

This generic dynamic behavior can now be rationalized in terms of the topology of the chemical bonding: fluctuations in *cold* clusters act only locally by breaking the Li–Li distance alternation while preserving the general bonding pattern (which is similar to the "shape-consistent distortion" of Li_8), whereas in *hot* clusters the bond topology in terms of multicenter bonds can be changed qualitatively (which is similar to the isomerization transformation of Li_8). As a result, the electronic properties of cold, thermalized clusters are essentially those of the most stable isomer *despite* the Li–Li distance equalization due to zero-point motion, whereas the spectra of hot clusters are expected to be a "thermal mixture" of those of electronically quite different individual isomers. Thus, electronic properties as manifest in optical spectra from thermalized cluster ensembles should be temperature dependent only at high temperatures and become invariant for sufficiently cold clusters.

Nanoscale clusters Li_{20} and Li_{40}—a step towards the bulk and surfaces

Up to this point only small "clusters" were analyzed so that all of the atoms could be classified to be part of the "surface" of the cluster, in that all the atoms display lower coordination numbers with respect to those found in the bulk phase. In the spirit of understanding chemical bonding in the bulk based on bonding in clusters, the cluster size has to be increased. For this program, the analysis, such as that presented in Figures 1 and 4, of many orbitals for these large C_1-symmetric clusters would be cumbersome, whereas the ELF yields easier access to bonding concepts. The largest clusters investigated here, Li_{20} and Li_{40}, are shown in Figure 6a and 6b, respectively. Like the smaller clusters these low-energy isomers consist of closely packed tetrahedral subunits and also feature short and long Li–Li distances: for instance see Figure 1b of ref. [39] for a distance distribution function. However, the location of the short Li–Li contacts is invariably found within the first two atomic layers from the surface, whereas those atoms within the center of the clusters are not involved in this type of bonding. These structural considerations imply that the electrons behave somehow differently in these two regions, but to what extent?

The valence electron density is distributed throughout the whole cluster, but largely confined to the cluster center, seeFigure 6c and 6d. The ELF behaves quite differently: the highest localization occurs at the *outside* of the cluster as clearly inferred from Figure 6e and 6f for Li_{20} and Li_{40}, respectively. Attractors with a localization maximum of $\eta^{max} \geq 0.9$ as known from the smaller clusters are *exclusively*

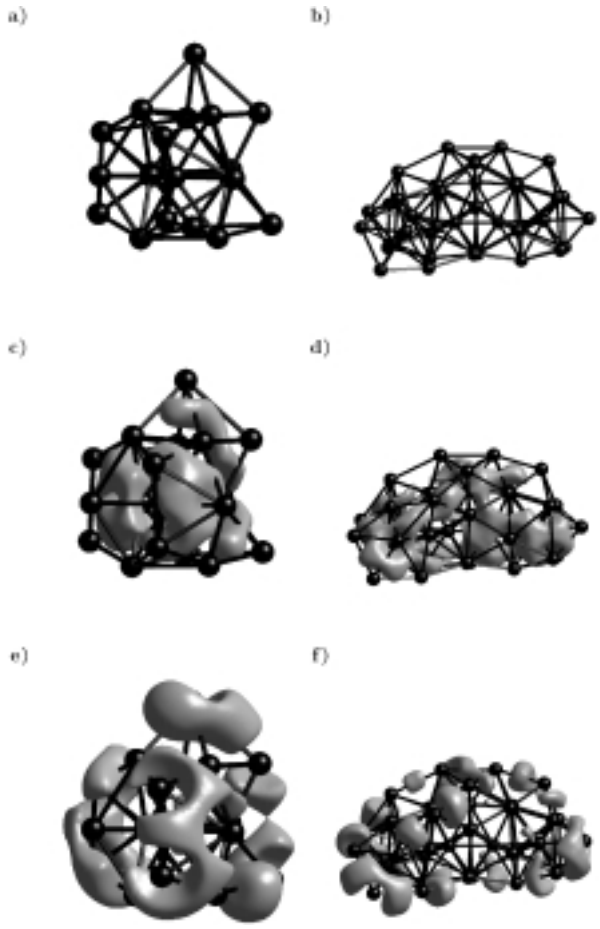

Figure 6. Structure of local minima of a) Li_{20} and b) Li_{40}. Density isosurfaces are depicted in c) and d) for $\rho^{iso} = 0.8\rho^{max}$ and ELF isosurfaces are shown in e) and f) for $\eta^{iso} = 0.85$ for Li_{20} and Li_{40}, respectively.

found on the surface, whereas the regions within the cluster have significantly lower values of $\eta^{max} \leq 0.7$ for both Li_{20} and Li_{40}. These η^{max} values are similar to those observed in solid lithium, in particular $\eta^{max} = 0.68$ for the bcc solid and $\eta^{max} = 0.72$ for the fcc phase (see the following section). This suggests that the center of the Li_{20} cluster, and even more so that of Li_{40}, has already begun to take on attributes similar to that of the bulk solid.

How does this situation arise? As seen so far the electrons tend to reside in interstitial regions as a result of the pπ-type component in the molecular wave function. The number of these interstitial regions relative to the number of electrons is small for the $n \leq 8$ atom Li_n clusters owing to the small number of atoms and low coordination numbers. The atoms within the center of the Li_{20} and Li_{40} clusters no longer exist in such a local chemical environment and experience coordination numbers as large as ten or twelve. Accompanying these nearest neighbors are also lots of interstitial regions over which electron pairs may be distributed that *qualitatively* should decrease the amount of electron pairs localized at any given region in space. Consequently, this is reflected in the ELF as a decrease in electron localization within the cluster center. In contrast, for the atoms on the cluster surface the bonding situation resembles that of the smaller clusters—hence the similar ELF. Thus, the cluster *surface* still retains

the bonding patterns found in the smaller species, whereas the electrons in the cluster core are much more delocalized. Yet, the clusters themselves have a "band gap" of approximately 1 eV and therefore cannot be classified as metallic. In conclusion, the Li_{20} and Li_{40} nanoclusters represent a scenario between a molecule and a metal. The inside of these species is characterized by low electronic localization similar to that of a metallic solid. The outside of these species is characterized by bonding similar to that in the smaller cluster and leads to localized surface states. These findings are interpreted as the onset of metallic character within the cluster core, which becomes readily apparent even for clusters as small as twenty atoms.

Solid lithium

Bulk lithium—the metallic bcc and fcc phases: How do these findings for clusters relate to the electronic structure of the bulk phases? First, the Li–Li distance alternation seen in clusters is found in none of the known phases of solid lithium: Li–Li distances of 3.04 Å and 3.12 Å have been reported for the bcc and fcc phases for instance, which classifies as "long" distances in the context of clusters. Furthermore, the system is metallic and thus the electrons must be more delocalized than in the clusters.

To probe this, the ELF of the (100) planes of bcc and fcc bulk lithium are displayed in Figure 7a and 7b, respectively. The ELF of both phases consists of attractors that are localized *in the center of octahedral cavities* formed by the six nearest-neighbor lithium atoms. The location of the octahedral attractors in the crystal is coincident with the maxima of the valence electron density (not shown). The η^{max} values for these octahedral attractors basins are 0.68 and 0.72 for the bcc and fcc phases, respectively. For the bcc phase, the basins are confluent already at $\eta^* \approx 0.66$ so that a channel-like network structure of the connected domains appears visually in the representation shown in Figure 7a. At variance with the bcc solid, the fcc phase exhibits a second smaller attractor basin within the tetrahedral holes, not visible in Figure 7b, with $\eta^{max} = 0.64$. These four-center attractor basins merges with the octahedral basins already at $\eta^{max} = 0.62$. This scenario is in qualitative agreement with previous findings.[12, 13, 58]

Superficially, this seems to be a unique situation from that of the smaller clusters in which electrons were localized within tetrahedra or triangles. This is also in contradiction with the conclusions regarding metallic phases as based on generalized valence-bond-theory calculations on three-dimensional clusters up to 13 atoms which suggest the electrons should be localized within tetrahedral sites of the fcc structure.[6] However, the present findings agree well with the generalized valence-bond description for the smaller clusters $n \leq 8$. Given that the surface to bulk ratio is large for such cluster sizes and the dramatic surface effects as demonstrated in previous section, it is unlikely that these small clusters provide an adequate representation of a bulk metallic solid. On the other hand, the ELF does coincide well with the observed η^{max} values found for the interior regions of the Li_{20} and Li_{40} clusters. This topology is reminiscent of multicenter bonding, in particular the six-center bonding as found in the cluster

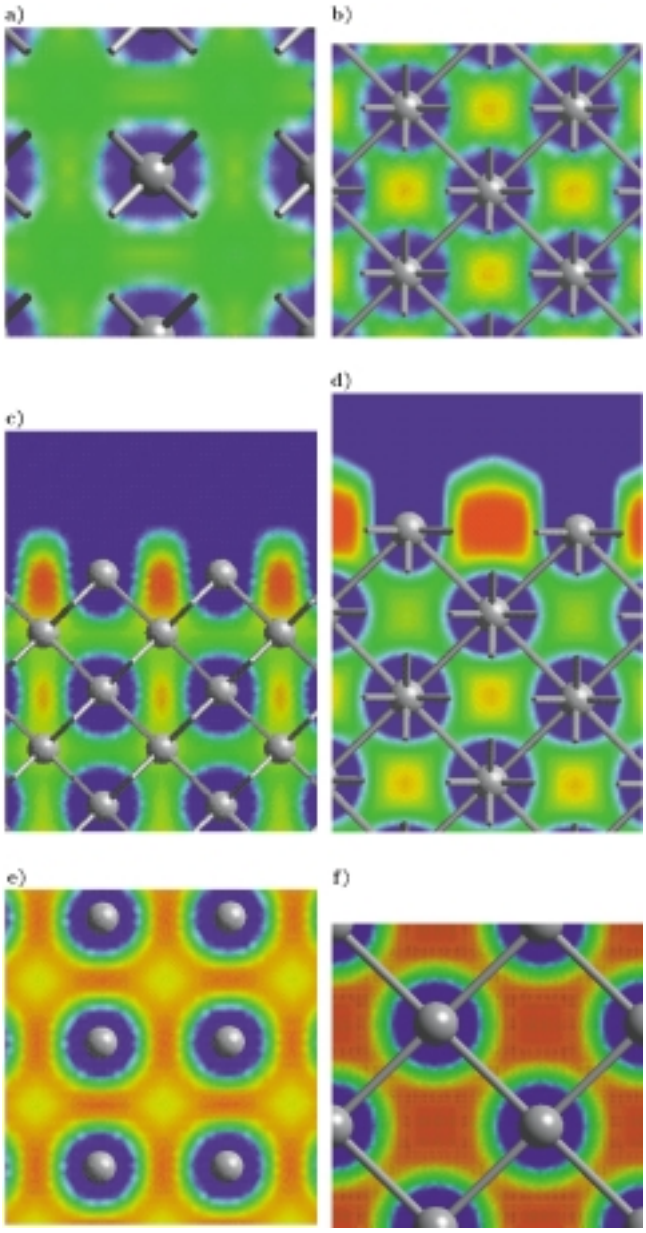

Figure 7. The ELF is shown as a contour slice through the (100) planes of the cubic cells of bcc and fcc metallic lithium solids in a) and b), respectively. This same plane is shown for the relaxed (001) surface of the bcc and fcc solids in c) and d), respectively. A contour slice in the plane of the surface atoms for the corresponding phases is shown in e) and f). Color of ELF contours: blue: $\eta \lesssim 0.5$; green: $\eta \approx 0.6$; yellow: $\eta \approx 0.7$; red: $\eta \gtrsim 0.75$.

study for three-dimensional structures, compare Figure 7a and 7b in particular with Figure 3c and 3d for D_{4h} Li_6 and C_s Li_8. These facts taken together suggest a similar origin that will allow us to establish the desired link between clusters and solid.

As in the smaller clusters, electrons are localized in interstitial regions in the bulk which have so far been ascribed to significant pπ-type interactions. It would be desirable to perform a similar analysis here as in the sections on Li_2 to Li_6 clusters, where insights into the ELF topology were gained by a complementary analysis based upon the canonical Kohn-Sham orbitals. However, this is impractical if one considers all of the over 125 orbitals that have been used in the present supercell calculations or the complex wavefunctions which

0947-6539/00/0616-2990 $ 17.50+.50/0 *Chem. Eur. J.* **2000**, *6*, No. 16

would arise when more then just the Γ point is used for Brillouin zone sampling in smaller supercells. This practical difficulty can be surmounted by examining the convergence of the ELF as a function of supercell size. Consider the fcc phase with a four atom cubic cell and the crystal orbitals obtained only at the Γ point. A single cubic fcc cell does not even qualitatively exhibit the same ELF as the larger $4\times4\times4$ supercell, but a $2\times2\times2$ supercell does. Thus, the crystal wavefunction is sufficiently converged for the purpose of *qualitative* analysis with only 16 orbitals.

In addition, this task may be reduced by invoking symmetry to the analysis of only a few symmetry-independent crystal orbitals. The $2\times2\times2$ supercell Γ point calculation corresponds to a Brillouin zone sampling for the four atom cubic cell at the following eight high-symmetry **k** points: Γ (0,0,0), X (½,0,0) (and its two symmetry equivalent points (0,½,0) and (0,0,½)), M (½,½,0) (and its two symmetry equivalent points (½,0,½) and (0,½,½)), and R (½,½,½); the indices in brackets are given with respect to the reciprocal vectors of the cubic cell. The orbitals upon which this discussion will depend are represented schematically in Figure 8; the R point generates no occupied orbitals and, therefore, need not be considered. There is only one occupied orbital with the symmetry of the Γ point, see the lower subpanel in Figure 8. This orbital is the lowest in energy and consists of an in-phase combination of s orbitals on each lattice site. Note the similarity with the lowest occupied orbital of the clusters in Figures 1 and 4. The next set of occupied orbitals is six-fold degenerate with symmetry

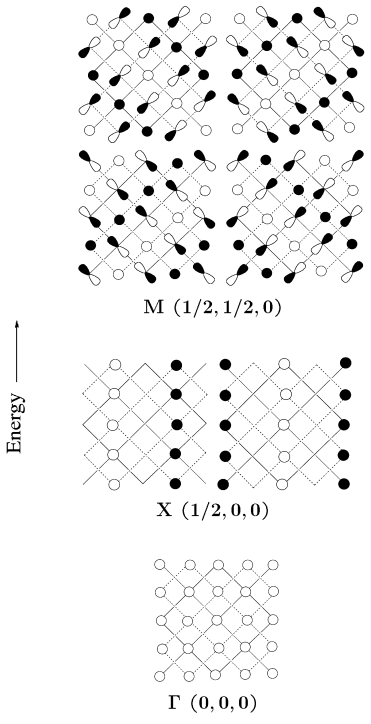

Figure 8. Schematic representation of the crystal orbitals of an fcc lattice of lithium as viewed down the (001) axis. Orbitals are shown at special points Γ (0,0,0), X (½,0,0) and M (½,½,0) from bottom to top, where the indices in the brackets refer to coordinates of the **k** vector with respect to reciprocal lattice vectors of the cubic cell. Solid (dashed) lines represent first nearest-neighbor contacts between atoms with height $z=0$ ($z=½$). Atoms are located at the intersection of two solid or two dashed lines (vertices). The centers of octahedral holes are located at the centers of the squares formed by solid (dashed) lines for $z=0$ ($z=½$).

corresponding to the X point and its two equivalent points, each of which contributes two orbitals; see the two center subpanels in Figure 8. These orbitals are almost entirely of s character and are nonbonding in the direction in which the phase of the reciprocal lattice vector is altered from 0 to ½, but remain bonding in the other two directions. The remaining occupied orbitals are part of a 12-fold degenerate set which have the symmetry of the M point or its symmetrical equivalents, where each point contributes four orbitals, see the upper four subpanels Figure 8. These contain both s-type and p-type character and, as for the clusters, show a pπ-bonding interaction between pairs of first-nearest neighbors; note that the upper and lower lobes of the partial π bonds lie within adjacent octahedral voids. This extra π character is operative in all first-nearest neighbor interactions due to the "isotropy" of the fcc or bcc solids. Thus, no particular bond is favored over others and no Li–Li distance alternation can result because of that. Moreover, the ELF acquires its maxima above and below the Li–Li connecting lines as in the clusters, that is, within the octahedral cavities. This is also found for the bcc phase with the exception that there are only eight bonds with partial π character that contribute to each attractor basin as opposed to the twelve in fcc.

As in the previous section a *qualitative* understanding of the observed increase in localization as one goes from the bcc ($\eta^{max}=0.68$) to the fcc ($\eta^{max}=0.72$) solid may be obtained by considering how the electron pairs are distributed in these two phases. There are three octahedral cavities in the two-atom cubic bcc cell but four in the four-atom cubic fcc cell. On first sight, there are more interstitial sites in the bcc lattice, that is, a ratio of ⅔ valence electrons per octahedral hole, whereas this ratio is larger, ≈1 electron per octahedral hole, for fcc. Thus, *qualitatively* one may expect that the electrons in bcc lithium will have a lower probability of being localized at any given point in space relative to those in the fcc or other close-packed phases. There is more space over which the electron pairs may be delocalized for the more open bcc solid as opposed to the fcc phase, a fact which is reflected by an increase in the η^{max} value for the latter.

In summary, the localization properties of the electrons in the bulk metallic phases are intimately tied to the p-orbital contribution to the wavefunction in extension to what is found in the cluster world. These new findings suggest that associated with the low-temperature phase transition from bcc to fcc and other close-packed phases[60] there is also a significant change in the localization properties of the electrons. The existence of these localization regimes with maxima that are substantially higher then the ELF value for the free-electron gas correlates well with the observation that Li is a "bad free-electron metal"[18, 19, 21] Finally, these results strongly suggest that the pπ interactions underly the recent prediction that solid lithium under high pressures undergoes a so-called "dimerization transition" thereby creating an anisotropic *Cmca* structure[61] with Li–Li distance alternation as found in the clusters. Furthermore, the results of section "Implications" hint that this feature may be radically affected at low temperatures due to averaging effects induced by zero-point motion, thus changing the *time-averaged* structure as observed in diffraction experiments, compare with refs. [25–29]

Lithium slabs—bcc and fcc (001) surfaces: What about the surface of metallic lithium solids? ELF is shown as a contour slice in the (100) plane in Figure 7c and 7d and as a slice parallel to the surface in Figure 7e and 7f for the (001) surfaces of bcc and fcc, respectively. It is found that the ELF has large attractor basins within the interstitial sites between the terminating atoms, which corresponds to the octahedral holes in the bulk, with $\eta^{max} \approx 0.80$ and 0.85 for bcc and fcc, respectively. With reference to the bulk, the maximum localization is strongly enhanced from 0.68 to 0.80 and from 0.72 to 0.85 for the bcc and fcc surfaces, respectively. These attractor basins are in the same location as those in the bulk except that the formation of the surface removes one of the vertices of the octahedral cavity. These basins become confluent into one large basin at about $\eta^* \approx 0.74$ for both surfaces, forming a pattern of interconnecting rings of high localization that is confined in two dimensions at the surface only. The values of η^* between these attractors and those in the lower layers is the same as in the bulk phase, that is, $\eta^* = 0.62$. The large range of the ELF scale over which the surface attractor basins remain independent both of each other and the basins within the bulk indicate that each may be thought of as an independent "dangling bonds".

The effect of increased electron localization is, as expected, not confined to the first layer as can be seen from the cuts in Figure 7c and 7d; the ELF is enhanced clearly also in lower layers of octahedral sites. The enhancement is most pronounced in the surface layer and decreases from atomic layer to atomic layer as one moves away from the surface. Each attractor basin below those directly on the surface is confluent with its neighbors in an identical way as the bulk. At a depth of about two atomic layers for fcc and four layers for bcc the attractor basins become identical with those in the bulk phase. The increase of localization in surface layers goes hand in hand with an increase in charge density, which is accumulated at the surface relative to the bulk (not shown).

For both surfaces there is essentially no relaxation occurring. The interlayer distance between those atoms at the surface and those within the second layer decreases by only about 0.01 Å; this corresponds to bond length changes of 0.01 Å and 0.02 Å shorter than those for the bulk bcc and fcc phases, respectively. Based on the discussion of in the section on implications above, it seems likely that these surface states, which are much more localized and also directional, induce an extra rigidity in the surface layer. Thus the network of dangling bonds, with the same periodicity as the bulk, will be less likely to distort and undergo surface relaxation.

Conclusions

Lithium bonding: The bonding properties of lithium were investigated as they evolve from molecules and small clusters to nanoclusters and finally to bulk phases including their surfaces. In accord with pioneering studies on that subject, three-center and four-center bonds were found to dominate the electronic structure of small clusters up to Li_5^+. After further investigations, our earlier finding of the existence of short and long Li–Li distances ("distance alternation") and its correlation with multicenter bonding is now rationalized. The clue comes from the well-known contribution of p-type orbitals. We have foubd that short Li–Li distances appear as a result of an additional stabilization due to the contribution of pπ interactions that act *in phase along certain directions*. In terms of structure, this stabilization amounts to a bond length contraction of roughly 0.4 Å, which corresponds to about 10%. In extreme situations this can lead to Li–Li distances which are shorter than that of the dimer!

An interesting question is related to the resistance of the Li–Li distance alternation with respect to fluctuations on the Born–Oppenheimer ground-state electronic surface. Using ab initio molecular dynamics and path-integral simulations, we showed previously that classical thermal fluctuations at 100 K or quantum zero-point motion of the relatively light lithium nuclei destroy the distance alternation in clusters completely, but do not lead to isomerization. The breakdown of the distance alternation can be understood in the light of the present bonding analysis. It is found that the topology of the electronic structure and, hence, the type of bonding does not change as a result of these fluctuations, whereas isomerizations would require changes in the bonding topology.

A novel feature appears in the ELF topology of the lowest energy (nonplanar D_{4h}) isomer of Li_6. This case, as well as isomers of Li_8, can be described in terms of six-center six-electron bonding. A similar multicenter motif was found to characterize the bonding in bcc bulk lithium: the ELF attractors were found to reside in the center of the octahedral interstitial holes, that is, the basin of most pronounced localization encompasses six atoms. In accordance with earlier findings, the channels connecting the multicenter attractors form a three-dimensional network of "flat paths" that wind through the interstitial space. This amounts to saying that metallic bulk lithium is best described in terms of multicenter bonds as a result of a crucial contribution of directional p-type interactions. However, in the case of "isotropic solids", such as bcc or fcc crystals, the Li–Li distance alternation cannot develop due to symmetry.

Finally, surface effects were considered in order to establish the connection between the behavior of small clusters and the bulk by using both large clusters and slabs. Nanoclusters that are comprised of 20 and 40 atoms, obtained after elaborate ab initio simulated annealing, feature an enhanced and anisotropic localization at their "surface"; this includes the occurrence of short Li–Li distances similar to those found in the small clusters. In contrast, their "core" region is characterized by ELF values quite close to those found in the bulk. Thus, a simple picture would be that these nanoclusters already share properties of bulk metallic lithium in the core region, whereas their surface electronic properties resembles those of smaller clusters. The (001) surfaces of the bcc and fcc bulk phases behave in a similar fashion to those of the nanoclusters in that a much stronger localization occurs close to the surface. This enhancement relaxes to the bulk value within two (fcc) to four (bcc) atomic layers. The topology of the octahedral attractor basins does not change qualitatively at the surface relative to the bulk, except that one vertex atom is removed from the octahedron. The resulting rigidity of these surfaces goes hand in hand with the observed, small surface relaxation.

0947-6539/00/0616-2992 $ 17.50+.50/0 *Chem. Eur. J.* **2000**, *6*, No. 16

There is a natural continuum in bonding properties as the number of atoms within the lithium assemblies grows. At all sizes p orbitals allow for the localization of electrons into interstitial regions, such as the centers of triangles, tetrahedra, or even octahedra. However, this is not the root cause of the metallic state in the bulk. The preference for delocalization of electrons becomes apparent even for Li_6 as its (nonplanar D_{4h}) ground state is also characterized by multicenter bonds. The bonding is at all sizes multicentered, but it is the presence of a large number of *unsaturated* multicenter bonds that ultimately leads to the metallic state of solid lithium.

Acknowledgements

It is a pleasure to acknowledge Jürg Hutter and Andreas Savin for helpful discussions.

[1] *Physics and Chemistry of Finite Systems: From Clusters to Crystals* (Eds.: P. Jena, S. N. Khanna, B. K. Rao), Kluwer, Dordrecht, **1992**; W. A. de Heer, *Rev. Mod. Phys.* **1993**, *65*, 611; *Clusters of Atoms and Molecules* (Ed.: H. Haberland), Springer, Berlin, **1994**; *Large Clusters of Atoms and Molecules* (Ed.: T. P. Martin), Kluwer, Dordrecht, **1996**.
[2] V. Bonačić-Koutecký, P. Fantucci, J. Koutecký, *Chem. Rev.* **1991**, *91*, 1035.
[3] P. Ballone, W. Andreoni in *Metal Clusters* (Ed.: W. Ekardt), Wiley, New York, **1999**.
[4] R. Hoffmann, *Solids and Surfaces—A Chemist's View of Bonding in Extended Systems*, VCH, New York, **1988**.
[5] D. Petifor, *Bonding and Structure of Molecules and Solids*, Clarendon, Oxford, **1995**.
[6] M. A. McAdon, W. A. Goddard III, *Phys. Rev. Lett.* **1985**, *55*, 2563; M. A. McAdon, W. A. Goddard III, *J. Non-Cryst. Solids* **1985**, *75*, 149; M. A. McAdon, W. A. Goddard III, *J. Phys. Chem.* **1987**, *91*, 2607.
[7] M.-W. Sung, R. Kawai, J. H. Weare, *Phys. Rev. Lett.* **1994**, *73*, 3552; R. Kawai, M. W. Sung, J. H. Weare in *Physics and Chemistry of Finite Systems: From Clusters to Crystals*, *Vol. 1* (Eds.: P. Jena, S. N. Khanna, B. K. Rao), Kluwer, Dordrecht, **1992**, p. 441.
[8] G. Gardet, F. Rogemond, H. Chermette, *J. Chem. Phys.* **1996**, *105*, 9933.
[9] C. Gatti, P. Fantucci, G. Pacchioni, *Theor. Chim. Acta* **1987**, *72*, 433; note that only "Part I: Planar Li_n clusters ($n = 4,5,6$)" of this study was published.
[10] A. D. Becke, K. E. Edgecombe, *J. Chem. Phys.* **1990**, *92*, 5397.
[11] A. Savin, A. D. Becke, J. Flad, R. Nesper, H. Preuss, H. G. von Schnering, *Angew. Chem.* **1991**, *103*, 421; *Angew. Chem. Int. Ed. Engl.* **1991**, *30*, 409.
[12] B. Silvi, A. Savin, *Nature* **1994**, *371*, 683.
[13] B. Silvi, C. Gatti, *J. Phys. Chem. A* **2000**, *104*, 947; see also http://surya.lct.jussieu.fr/silvi/metal/english.html for color three-dimensional renderings of ELF for bcc solid lithium.
[14] J. R. Mohallem, R. O. Vianna, A. D. Quintão, A. C. Pavão, R. McWeeny, *Z. Phys. D* **1997**, *42*, 135; see also A. D. Quintão, R. O. Vianna, J. R. Mohallem, *Eur. Phys. J. D* **1999**, *6*, 89.
[15] O. Sugino, H. Kamimura, *Mat. Sci. Eng. B* **1989**, *3*, 443; O. Sugino, H. Kamimura, *Phys. Rev. Lett.* **1990**, *65*, 2696.
[16] P. Blaise, F. Spiegelmann, D. Maynau, J. P. Malrieu, *Phys. Rev. B* **1990**, *41*, 5566.
[17] R. Rousseau, D. Marx, *Phys. Rev. A* **1997**, *56*, 617.
[18] Y. Sakurai, Y. Tanaka, A. Bansil, S. Kaprzyk, A. T. Stewart, Y. Nagashima, T, Hyodo, S. Nanao, H. Kawata, N. Shiotani, *Phys. Rev. Lett.* **1995**, *74*, 2252.
[19] W. Schülke, G. Stutz, F. Wohlert, A. Kaprolat, *Phys. Rev. B* **1996**, *54*, 14381.
[20] M. M. Dacorogna, M. L. Cohen, *Phys. Rev. B* **1986**, *34*, 4996.
[21] A. Y. Liu, M. L. Cohen, *Phys. Rev. B* **1991**, *44*, 9678.
[22] M. Sigalas, N. C. Bacalis, D. A. Papaconstantopoulos, M. J. Mehl, A. C. Switendick, *Phys. Rev. B* **1990**, *42*, 11637.
[23] G. Yao, J. G. Xu, X. W. Wang, *Phys. Rev. B* **1996**, *54*, 8393.
[24] A. Heilingbrunner, G. Stollhoff, *J. Chem. Phys.* **1993**, *99*, 6799.
[25] N. W. Ashcroft, *Phys. Rev. B* **1989**, *39*, 10552.
[26] N. Tugluoglu, R. H. Mutlu, *Phys. Rev. B* **1996**, *54*, 10253; Erratum: N. Tugluoglu, R. H. Mutlu, *Phys. Rev. B* **1997**, *56*, 12651.
[27] P. Staikov, A. Kara, T. S. Rahman, *J. Phys. Condens. Matter* **1997**, *9*, 2135.
[28] C. Filippi, D. M. Ceperley, *Phys. Rev. B* **1998**, *57*, 252.
[29] K. Doll, N. M. Harrison, V. R. Saunders, *J. Phys. Condens. Matter* **1999**, *11*, 5007.
[30] W. H. Gerber, E. Schumacher, *J. Chem. Phys.* **1978**, *69*, 1692.
[31] J. L. Martins, R. Car, J. Buttet, *J. Chem. Phys.* **1983**, *78*, 5646.
[32] P. Ballone, P. Milani, *Phys. Rev. B* **1992**, *45*, 11222 .
[33] R. Kawai, J. F. Tombrello, J. H. Weare, *Phys. Rev. A* **1994**, *49*, 4236.
[34] J. Jellinek, V. Bonačić-Koutecky', P. Fantucci, M. Wiechert, *J. Chem. Phys.* **1994**, *101*, 10092; P. Fantucci, V. Bonačić-Koutecký, J. Jellinek, M. Wiechert, R. J. Harrison, M. F. Guest, *Chem. Phys. Lett.* **1996**, *250*, 47; V. Bonačić-Koutecký, J. Jellinek, M. Wiechert, P. Fantucci, *J. Chem. Phys.* **1997**, *107*, 6321; D. Reichardt, V. Bonačić-Koutecký, P. Fantucci, J. Jellinek, *Chem. Phys. Lett.* **1997**, *279*, 129.
[35] R. O. Jones, A. I. Lichtenstein, J. Hutter, *J. Chem. Phys.* **1997**, *106*, 4566.
[36] D. A. Gibson, E. A. Carter, *Chem. Phys. Lett.* **1997**, *271*, 266.
[37] D. Marx, M. Parrinello, *Z. Phys. B* **1994**, *95*, 143.
[38] D. Marx, M. Parrinello, *J. Chem. Phys.* **1996**, *104*, 4077; M. E. Tuckerman, D. Marx, M. L. Klein, M. Parrinello, *J. Chem. Phys.* **1996**, *104*, 5579.
[39] R. Rousseau, D. Marx, *Phys. Rev. Lett.* **1998**, *80*, 2574.
[40] R. Rousseau, D. Marx, *J. Chem. Phys.* **1999**, *111*, 5091.
[41] R. O. Weht, J. Kohanoff, D. A. Estrin, C. Chakravarty, *J. Chem. Phys.* **1998**, *108*, 8848.
[42] M. Broyer, J. Chevaleyre, Ph. Dugourd, J. P. Wolf, L. Wöste, *Phys. Rev. A* **1990**, *42*, 6954; J. Blanc, M. Broyer, J. Chevaleyre, Ph. Dugourd, H. Kühling, P. Labastie, M. Ulbricht, J. P. Wolf, L. Wöste, *Z. Phys. D* **1991**, *19*, 7; Ph. Dugourd, J. Blanc, V. Bonačić-Koutecký, M. Broyer, J. Chevaleyre, J. Koutecký, J. Pittner, J. P. Wolf, L. Wöste, *Phys. Rev. Lett.* **1991**, *67*, 2638; J. Blanc, V. Bonačić-Koutecký, M. Broyer, J. Chevaleyre, Ph. Dugourd, J. Koutecký, C. Scheuch, J. P. Wolf, L. Wöste, *J. Chem. Phys.* **1992**, *96*, 1793.
[43] B. K. Rao, P. Jena, A. K. Ray, *Phys. Rev. Lett.* **1996**, *76*, 2878.
[44] A. Rubio, J. A. Alonso, X. Blase, L. C. Balbás, S. G. Louie, *Phys. Rev. Lett.* **1996**, *77*, 247.
[45] R. G. Parr, W. Yang, *Density-Functional Theory of Atoms, Molecules*, Oxford University Press, Oxford, **1989**; R. O. Jones, O. Gunnarsson, *Rev. Mod. Phys.* **1989**, *61*, 689.
[46] J. P. Perdew, A. Zunger, *Phys. Rev. B* **1981**, *23*, 5048.
[47] A. D. Becke, *Phys. Rev. A* **1988**, *38*, 3098.
[48] N. Troullier, J. L. Martins, *Phys. Rev. B* **1991**, *43*, 1993.
[49] S. G. Louie, S. Froyen, M. L. Cohen, *Phys. Rev. B* **1982**, *26*, 1738.
[50] J. Hutter, P. Ballone, M. Bernasconi, P. Focher, E. Fois, St. Goedecker, D. Marx, M. Parrinello, M. Tuckerman, *CPMD Version 3.0*, Max-Planck-Institut für Festkörperforschung, IBM Zurich Research Laboratory **1995–96**.
[51] R. Car, M. Parrinello, *Phys. Rev. Lett.* **1985**, *55*, 2471.
[52] *Pearson's Handbook of Crystallographic Data for Intermetallic Phases* (Eds.: P. Villars, L. D. Calvert), American Society of Metals, Metals Park Ohio, **1985**.
[53] D. Marx, A. Savin, *Angew. Chem.* **1997**, *109*, 2168; *Angew. Chem. Int. Ed. Engl.* **1997**, *36*, 2077.
[54] A. Savin, R. Nesper, S. Wengert, T. F. Fässler, *Angew. Chem.* **1997**, *109*, 1892; *Angew. Chem. Int. Ed. Engl.* **1997**, *36*, 1808.
[55] T. F. Fässler, A. Savin, *Chem. Unserer Zeit* **1997**, *31*, 110.
[56] R. F. W. Bader, S. Johnson, T.-H. Tang, P. L. A. Popelier, *J. Phys. Chem.* **1996**, *100*, 15398.
[57] J. K. Burdett, T. A. McCormick, *J. Phys. Chem. A* **1998**, *102*, 6366.
[58] A. Savin, O. Jepsen, J. Flad, O. K. Andersen, H. Preuß , H. G. von Schnering, *Angew. Chem.* **1992**, *104*, 186; *Angew. Chem. Int. Ed. Engl.* **1992**, *31*, 187.
[59] W. L. Cao, C. Gatti, P. J. MacDougall, R. F. W. Bader, *Chem. Phys. Lett.* **1987**, *141*, 380; G. I. Bersuker, C. Peng, J. E. Boggs, *J. Phys. Chem.* **1993**, *97*, 9323; M. Challacombe, J. Cioslowski, *Chem. Phys. Lett.* **1994**, *224*, 179.
[60] W. Schwarz, O. Blaschko, *Phys. Rev. Lett.* **1990**, *65*, 3144.
[61] J. B. Neaton, N. W. Ashcroft, *Nature* **1999**, *400*, 141.

Received: January 17, 2000 [F2243]